Cell Reports
Article

mTORC1 Targets the Translational Repressor 4E-BP2, but Not S6 Kinase 1/2, to Regulate Neural Stem Cell Self-Renewal In Vivo

Nathaniel W. Hartman,[1,2] Tiffany V. Lin,[1] Longbo Zhang,[1] Grace E. Paquelet,[1] David M. Feliciano,[1] and Angélique Bordey[1,*]
[1]Departments of Neurosurgery, and Cellular and Molecular Physiology, Yale University School of Medicine, New Haven, CT 06520-8082, USA
[2]Present address: Natural Sciences and Mathematics, The Richard Stockton College of New Jersey, Galloway, NJ 08205, USA
*Correspondence: angelique.bordey@yale.edu
http://dx.doi.org/10.1016/j.celrep.2013.09.017

SUMMARY

The mammalian target of rapamycin complex 1 (mTORC1) integrates signals important for cell growth, and its dysregulation in neural stem cells (NSCs) is implicated in several neurological disorders associated with abnormal neurogenesis and brain size. However, the function of mTORC1 on NSC self-renewal and the downstream regulatory mechanisms are ill defined. Here, we found that genetically decreasing mTORC1 activity in neonatal NSCs prevented their differentiation, resulting in reduced lineage expansion and aborted neuron production. Constitutive activation of the translational repressor 4E-BP1, which blocked cap-dependent translation, had similar effects and prevented hyperactive mTORC1 induction of NSC differentiation and promoted self-renewal. Although 4E-BP2 knockdown promoted NSC differentiation, p70 S6 kinase 1 and 2 (S6K1/S6K2) knockdown did not affect NSC differentiation but reduced NSC soma size and prevented hyperactive mTORC1-induced increase in soma size. These data demonstrate a crucial role of mTORC1 and 4E-BP for switching on and off cap-dependent translation in NSC differentiation.

INTRODUCTION

Neural stem cells (NSCs) lie at the core of brain development and repair, and alterations in NSC self-renewal and differentiation can have major consequences on brain function at any stage of life (Gage, 2000). As a result, a series of extracellular signals tightly regulates NSC self-renewal and differentiation at different stages of brain development (Shi et al., 2008). Many of these extracellular signals subsequently activate the mammalian target of rapamycin complex 1 (mTORC1) signaling pathway, which is an intracellular hub of translational regulation (Tee and Blenis, 2005; Laplante and Sabatini, 2012). mTORC1 is of particular interest because it is dysregulated and most often hyperactive in several neurodevelopmental disorders associated with neurocognitive and psychiatric impairments, such as tuberous sclerosis complex, fragile X syndrome, and autism spectrum disorder (Inoki et al., 2005; Hoeffer et al., 2012; Hoeffer and Klann, 2010; Santini and Klann, 2011; Wang and Doering, 2013).

Despite a wealth of studies related to the impact of hyperactive mTORC1 on brain development in vivo and to some extent NSC behavior in vitro (Magri et al., 2011; for review, see Feliciano et al., 2013b; Magri and Galli, 2013), very little is known about the physiological function of mTORC1 on NSC self-renewal and neuron production in vivo. mTORC1 function has been examined using a pharmacological approach by injecting the mTOR blocker rapamycin, either alone or in conjunction with a ligand that activates the mTORC1 pathway (Paliouras et al., 2012; Magri and Galli, 2013). Rapamycin is important to test because of its clinical value to treat disorders associated with hyperactive mTORC1 activity, such as tuberous sclerosis complex (Ehninger and Silva, 2011), but it does not distinguish cell-autonomous from non-cell-autonomous effects and may also block mTOR complex 2. Adding to our knowledge gap is the lack of information related to the direct downstream effectors mediating hyperactive mTORC1 effects on NSC self-renewal. Addressing this issue is of high fundamental and clinical significance for identifying novel therapeutic targets to prevent the negative effects of hyperactive mTORC1 on NSCs in several neurodevelopmental disorders, as well as in aging (Lamming et al., 2013; Johnson et al., 2013; Inoki et al., 2005).

Here, we explore mTORC1 and its downstream effectors' function on neonatal NSCs in the subventricular zone (SVZ), a neurogenic niche that confers a high degree of plasticity for circuit remodeling and repair after birth (Mitchell et al., 2004; Sanai et al., 2011; Feliciano et al., 2012). In vivo electroporation in neonates was used to transfect expression or knockdown vectors selectively in NSCs lining the lateral wall of the lateral ventricle and manipulate the activity of mTORC1 and its downstream effectors, the translational repressors 4E-BPs and

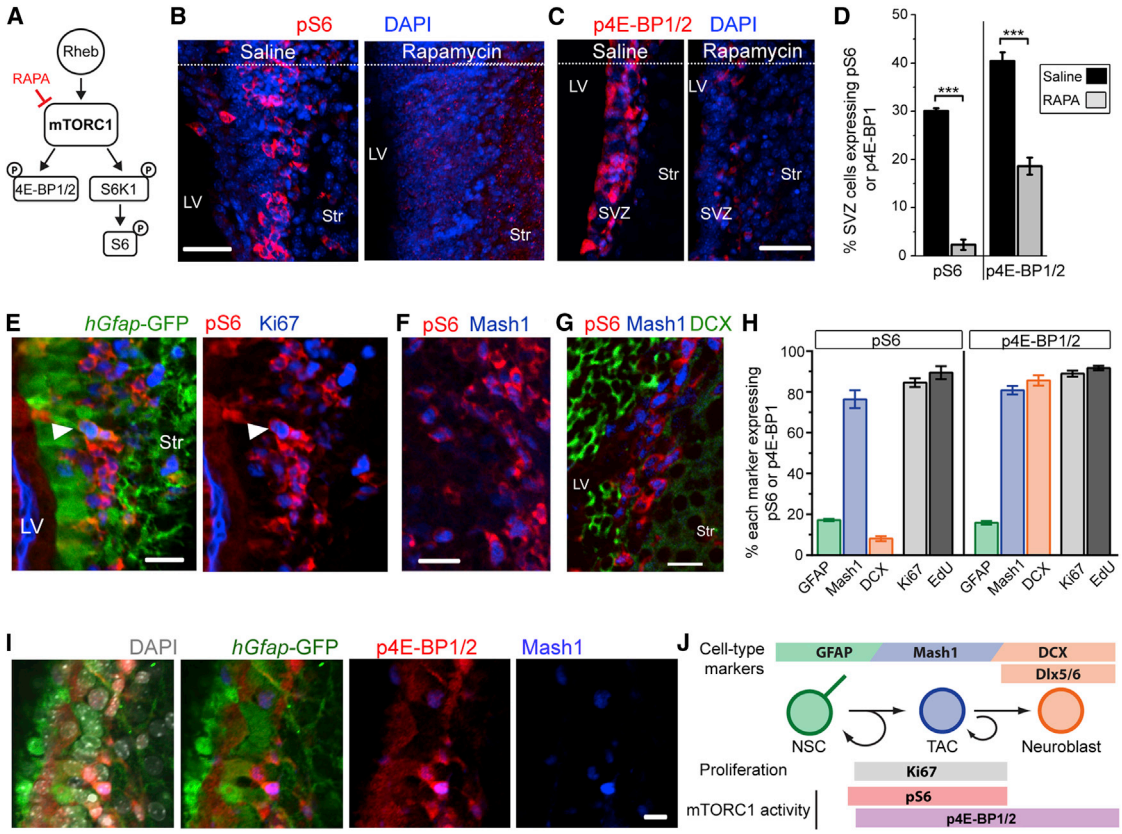

Figure 1. Basal Level of mTORC1 Activity in Proliferative NSCs and TACs in the Neonatal SVZ

(A) Diagram illustrates Rheb-mTORC1 signaling pathway. Rapamycin (RAPA) blocks mTORC1 activity.

(B and C) pS6 immunostaining (S240/S244, red in B) or p4E-BP1/BP2 immunostaining (red in C) with DAPI (blue) counterstain is shown in coronal sections containing the SVZ along the lateral side of the lateral ventricle (LV) from a P9 mouse. Rapamycin was given at 0.5 mg/kg every 2 days from P5 to P9. Str, striatum. Scale bars, 70 μm.

(D) Bar graphs show the percentage (%) of SVZ cells expressing pS6 and p4E-BP1/BP2 at P9 under control and following rapamycin treatment (n = 4 mice for each condition). Asterisks indicate statistical significance (***$p < 0.001$) by Student's t test.

(E) Immunostaining is shown for Ki67 (blue) and pS6 (red), and GFP (green) in the SVZ of a coronal section of a P9 *hGFAP*-GFP mouse. The solid arrowheads point to pS6 expression in a GFP+ cell.

(F) Immunostaining is presented for pS6 (red) and Mash1 (blue) in the SVZ of a P9 coronal section.

(G) Immunostaining is shown for pS6 (red), Mash1 (blue), and DCX (green) in the SVZ of a P9 coronal section.

(H) Bar graphs show the percentage (%) of each cell population expressing pS6 and p4E-BP1/BP2.

(I) Immunostaining is shown for p4E-BP1/BP2 (red), Mash1 (blue), and GFP (green) with DAPI (gray) counterstain in the SVZ of a coronal section of a P9 *hGFAP*-GFP mouse.

(J) Diagram illustrates cell lineage in the neonatal SVZ and the cellular distribution of proliferative marker Ki67 and active mTORC1 effectors, p4E-BP1/BP2 and pS6.

Scale bars, 20 μm (E–G and I). Error bars indicate SEM (n = 3–4 mice for staining and analysis). See also Figure S1.

S6K1/S6K2. We found that decreasing mTORC1 activity prevented the generation of intermediate progenitors, leading to reduced neuron production. Consistent with this finding, increasing mTORC1 activity did not induce NSC proliferation but induced its terminal differentiation into highly proliferative intermediate progenitors, leading to an apparent increase in the number of proliferative cells. The hyperactive mTORC1 effect was mediated by inhibition of 4E-BP2, but not S6K1/S6K2, and activation of cap-dependent translation in regulating NSC self-renewal. These findings suggest that altering mTORC1 activity in NSCs affects neuron production and density that may lead to circuit instability.

RESULTS

mTORC1 Is Active in Proliferative NSCs and TACs in the Neonatal SVZ

To examine basal mTORC1 activity in NSCs, we immunostained the neurogenic SVZ on postnatal day 8 (P8)–P9 for phosphorylated 4E-BP1/BP2 (p4E-BP1/BP2) and phosphorylated ribosomal protein S6 (pS6, Serine [S] 240/244), which are both readouts of mTORC1 activity (Laplante and Sabatini, 2012) (Figures 1A–1C). In the SVZ, NSCs self-renew and generate transit-amplifying cells (TACs) that are highly proliferative and contribute to neuronal lineage amplification and neuroblast generation

(Figure 1J) (Merkle and Alvarez-Buylla, 2006). The SVZ can be divided into three regions, dorsal, lateral, and ventral (Figure S1A), which display different distributions of the different cell types (Figure S1B). For consistency, analysis was performed in the lateral SVZ. We found that p4E-BP1/BP2 and pS6 were expressed in a subset of SVZ cells, the percentage of which was significantly reduced by treatment with the mTORC1 blocker rapamycin (Figures 1B–1D), validating the mTORC1 dependence of these signals. Among the different cell types, proliferative (Ki67+) NSCs identified by expression of GFP driven by the human glial fibrillary acidic protein (*hGfap*) promoter (Pastrana et al., 2009) expressed pS6 (Figures 1E and 1H). The majority of TACs (75%) identified by expression of Mash1 (Parras et al., 2004) and ~10% of neuroblasts identified by doublecortin (DCX) expression immunostained positive for pS6 (Figures 1F–1H and S1B). The cellular distribution of p4E-BP1/BP2 was similar to that of pS6 except for neuroblasts, the majority of which expressed p4E-BP1/BP2 (Figures S1C and S1D). These findings are summarized in a diagram in Figure 1J.

Reduction of mTORC1 Activity in NSCs and TACs Limits Neuron Production

To investigate the function of mTORC1 on neuron production in vivo, we used in vivo neonatal electroporation. P0 littermate pups were transfected with a conditional plasmid encoding a small hairpin RNA (shRNA) directed against Ras homolog enriched in brain (Rheb), a direct activator of mTORC1, or encoding a control-scrambled shRNA (Lacar et al., 2010; Boutin et al., 2008; Chesler et al., 2008) (Figures 2A and 2B). The cells targeted by electroporation were quiescent and proliferative NSCs along the lateral wall of the lateral ventricle. Once in NSCs, plasmids were passed on to their progeny, TACs and neuroblasts, which migrate to their final location (i.e., the olfactory bulb [OB]) in about 2 weeks (Figures 2A and 2C). To induce shRNA expression constitutively, we coelectroporated the conditional shRNA constructs with a Cre recombinase (Cre)-encoding plasmid (pCAG-Cre, Figure 2B). A plasmid encoding the red fluorescent protein tdTomato (pCAG-RFP) was included as a reporter to label cells, resulting in coelectroporation of three vectors. Coelectroporation of three (pCAG-RFP plus pCAG-GFP plus pCAG-BFP, blue fluorescent protein) and two vectors resulted in 86.2% ± 1.2% and 94.4% ± 0.7% colocalization per cell, respectively (mean ± SEM, n = 3 mice each, Figures S2A and S2B, images for two vectors), resulting in an underestimation of reported effects by 14% and 6%, respectively. Two weeks following electroporation with control shRNA, RFP+ neurons born from transfected NSCs in the SVZ had migrated into the OB as expected (Figure 2D) (Lacar et al., 2010; Platel et al., 2010). Rheb knockdown led to decreased mTORC1 activity in transfected Neuro2a cells in vitro as well as in transfected SVZ cells and newborn OB neurons in vivo (Figures S2C–S2I). Decreased mTORC1 activity resulted in a significant 40% reduction in the density of RFP-expressing neurons in the OB (Figures 2D and 2E). To ensure that the reduction in newborn neurons was not due to alteration of neuroblast development, we knocked down mTORC1 activity specifically in neuroblasts. To do this, the conditional Rheb shRNA vector was used in *Dlx5/Dlx6*-Cre mice because Dlx5/Dlx6 expression is restricted to neuroblasts in this system (Figures 2F–2H) (Kohwi et al., 2007). The conditional shRNA vector contains a floxed GFP (see diagram in Figure 2B), which is expressed in transfected SVZ cells, but is lost in newborn neurons following GFP excision in *Dlx5/Dlx6*-Cre-expressing neuroblasts (Figures 2G and 2H). In addition, cotransfection of a conditional RFP demonstrated efficient Cre-mediated recombination in newborn neurons (Figure 2H). In *Dlx5/Dlx6*-Cre mice, decreased mTORC1 activity in neuroblasts did not alter the number of newborn neurons in the OB (Figures 2I and 2J). Collectively, these data suggest that mTORC1 activity in the SVZ controls NSC self-renewal or TAC proliferation and, therefore, regulates the production of newborn neurons.

mTORC1 Activity Is Required for TAC Generation

To determine whether mTORC1 acted on NSC self-renewal or TAC proliferation, we electroporated Rheb shRNA in NSCs at P0 and quantified total and proliferative TACs in the SVZ as a proportion of transfected cells at 3 and 7 days postelectroporation (DPE). Immunostaining was performed using an Alexa 633-conjugated secondary antibody (pseudocolored green in Figure 3) allowing us to distinguish the staining from GFP and RFP-labeled cells. By 3 DPE, proliferative NSCs transfected with the control shRNA generated Mash1+ TACs (Figure 3B). Rheb knockdown led to a significant ~60% decrease in the percentage of transfected cells expressing Mash1 (Figures 3B, 3D, and S3B at 7 DPE). There was also a 50% decrease in the percentage of transfected cells expressing Ki67 (Figures 3C–3F, S3A, and S3B at 7DPE), but no change in the proportion of transfected TACs expressing Ki67 or EdU (Figures 3E and 3F), suggesting that Rheb knockdown did not affect TAC proliferation. The Rheb knockdown effect was mTORC1 dependent because it was reproduced by a shRNA directed to Raptor, a necessary mTOR binding partner in mTORC1 (Figures 3G and S3C–S3F), and by pharmacological inhibition of mTORC1 activity with rapamycin (Figures 3H–3K). In addition, consistent with mTORC1's role as a master regulator of cell growth, Rheb knockdown resulted in a significant 17% decrease in the soma size of transfected NSCs (±4 SEM; $p < 0.05$, Student's t test; n = 3 mice each; data not shown). Collectively, these results suggest that baseline mTORC1 activity is required for Mash1+ TAC generation from NSCs.

mTORC1 Drives NSC Differentiation at the Expense of Self-Renewal

Because mTORC1 activity is upregulated in several neurological diseases (Chong et al., 2010), we explored the outcome of increasing mTORC1 activity by expressing a constitutively active Rheb ($Rheb^{CA}$) into NSCs at P0 (Figure 4) (Lafourcade et al., 2013; Maehama et al., 2008). As controls, littermates were electroporated with pCAG-GFP vector. Both conditions were coelectroporated with GFP (pCAG-GFP) as a reporter. Although the control condition has GFP, we injected additional pCAG-GFP to match the plasmid concentration between the two conditions. $Rheb^{CA}$ expression led to a significant increase in the percentage of transfected SVZ cells expressing pS6 at 3 DPE that was rapamycin sensitive, indicating mTORC1 activation (Figures S4A and S4B). We then found that $Rheb^{CA}$-induced

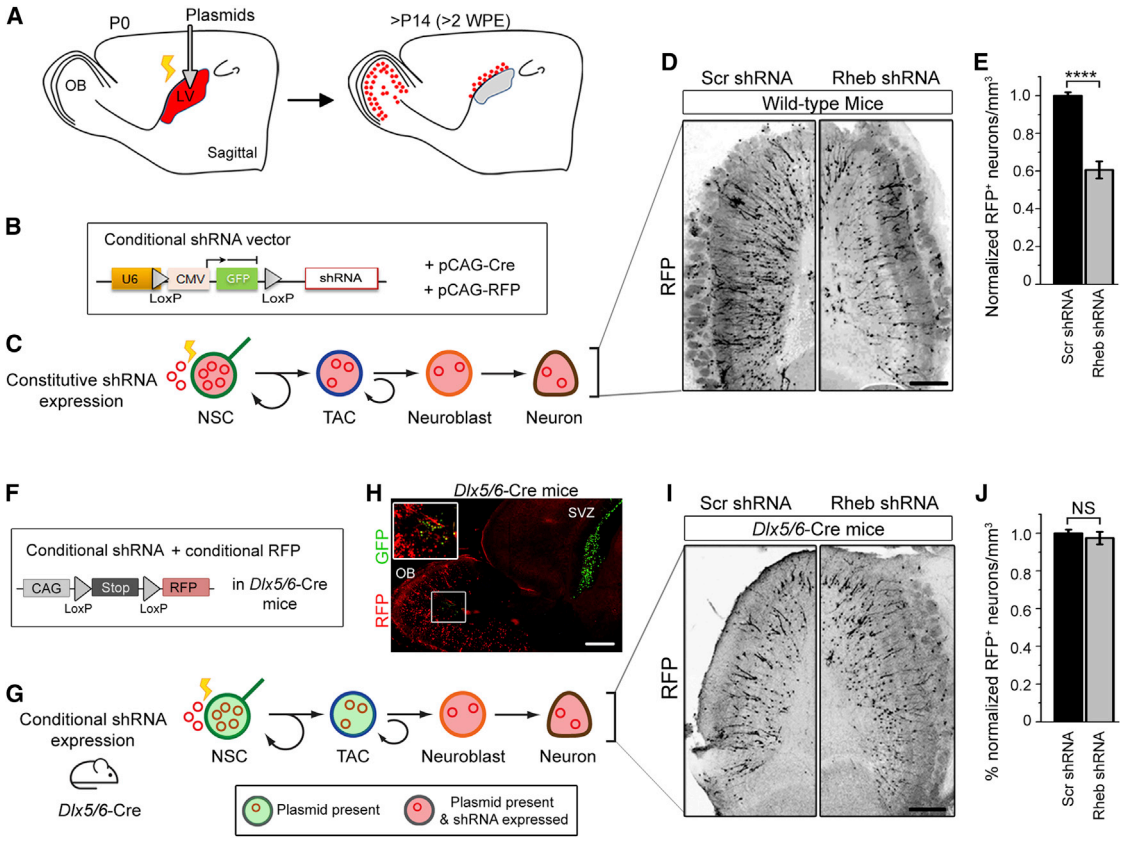

Figure 2. Genetically Decreasing mTORC1 Activity in NSCs and Mash1+ TACs Leads to Decreased Neuron Production

(A) Diagram illustrates neonatal electroporation at P0 in NSCs of the SVZ along the lateral side of the lateral ventricle and subsequent integration of plasmid-containing neurons in the OB by 2 weeks postelectroporation (WPE). The yellow symbol illustrates current injection.

(B) Vectors used in (C)–(E) in wild-type mice are shown.

(C) Diagram illustrates that plasmids are electroporated into NSCs and passed on to their daughter cells.

(D) Images present hemisected coronal OB sections containing neurons with RFP and scrambled (Scr) or Rheb shRNA in wild-type mice.

(E) Bar graphs show the corresponding percentage (%) of normalized RFP+ cells in the OB with Scr shRNA (black) or Rheb shRNA (gray). Asterisks indicate statistical significance (****$p < 0.0001$) by Student's t test.

(F) Vectors used in (G)–(J) in wild-type mice are presented.

(G) Diagram shows that electroporation of a conditional Cre-Lox shRNA and RFP vector results in Rheb shRNA and RFP expression selectively in neuroblasts in *Dlx5/Dlx6*-Cre mice.

(H) Image presents a sagittal section containing GFP+ cells (GFP from pSico vector) in the SVZ and RFP+ cells (RFP from the conditional RFP reporter) in the OB at 14 DPE in *Dlx5/Dlx6*-Cre mice. Cells acquire RFP upon Cre excision of the LoxP GFP cassette in neuroblasts known to express Dlx5/Dlx6 and progressively lose GFP surrounded by LoxP sites in the conditional shRNA vector. The migratory route from the SVZ to OB is not visible in this section. Inset is a zoom of RFP+ and GFP+ cells in the RMS of the OB.

(I and J) Images show hemisected OB sections (I) and normalized bar graphs of electroporated neurons (J) as in (D) and (E), but in *Dlx5/Dlx6*-Cre mice. NS, not significant.

Scale bars, 100 μm (D and I) and 200 μm (H). Error bars indicate SEM (n = 3–4 mice for staining and analysis). See also Figure S2.

increased mTORC1 activity in NSCs had opposite effects to those observed with Rheb knockdown. At both 3 and 7 DPE, there was a significant increase in the percentages of Rheb^{CA}-transfected cells expressing Mash1 and Ki67 (Figures 4A–4C and S4C–S4E at 7 DPE). The effect of Rheb^{CA} expression was due to mTORC1 activity because it was prevented by rapamycin treatment (Figure 4C).

The effect of hyperactive mTORC1 on NSCs could be explained by either causing quiescent NSCs to proliferate and generate TACs cells or inducing NSC differentiation into two TACs at the expense of self-renewal. To distinguish NSCs from their daughter cells, we quantified the proliferative index of NSCs in the SVZ in *hGfap*-GFP mice (Platel et al., 2009). The lack of increase in the Ki67 proliferative index of Rheb^{CA}-transfected NSCs at 3 DPE argues against an increase in NSC proliferation with hyperactive mTORC1 (Figure 4D). To further investigate Rheb^{CA} effect on NSC self-renewal, we examined the clonal behavior of NSCs in vitro. NSCs were transfected in vivo with RFP and Rheb^{CA} or a control GFP vector prior to plating as an adherent single-cell culture (Figure 4E). At 1 day in vitro (DIV), RFP+ cells were found as single cells, with 93%–95% immunostaining positive for GFAP, but not for Mash1, in

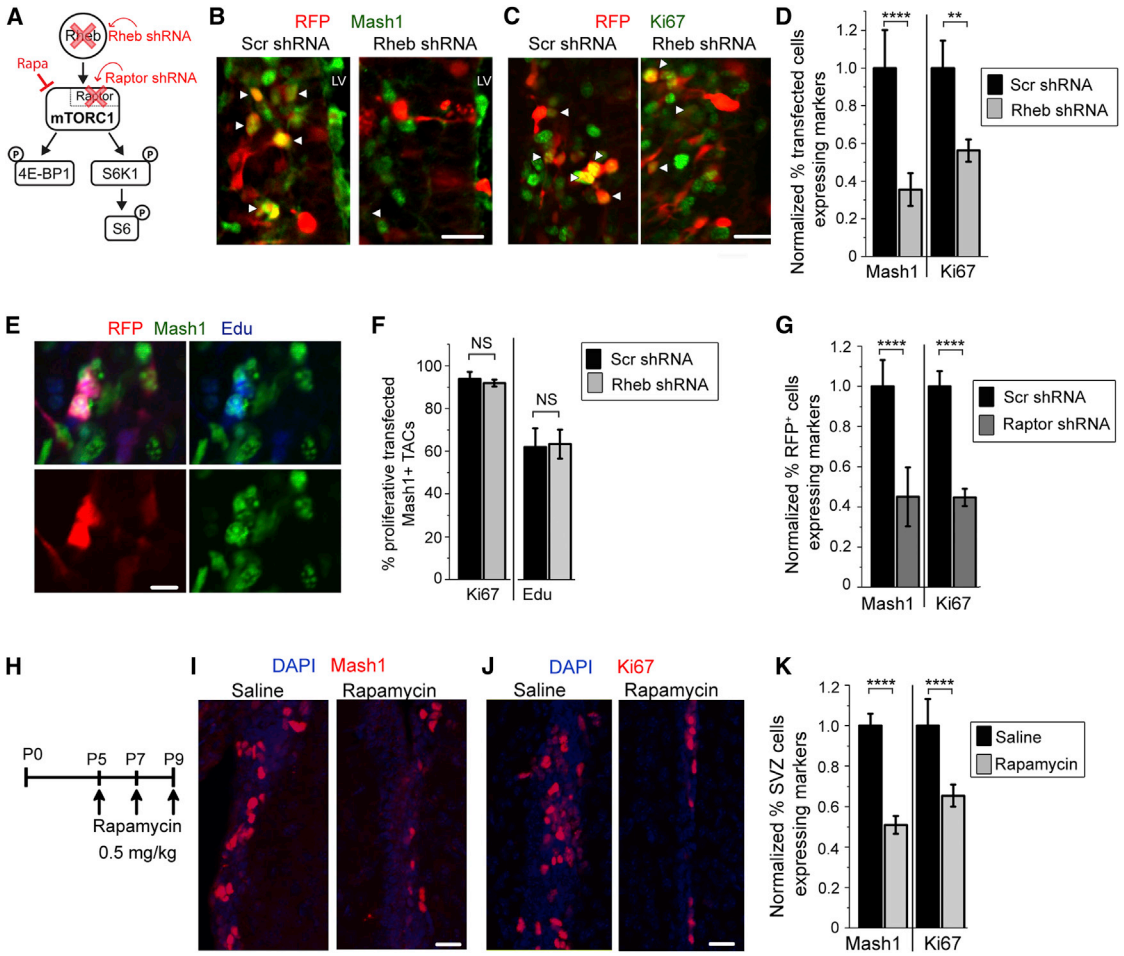

Figure 3. Baseline mTORC1 Activity Is Required for Mash1+ TAC Generation from NSCs

(A) Diagram illustrates Rheb-mTORC1 signaling pathway, in which Raptor is a component of mTORC1 and necessary for its activity. Rheb directly activates mTORC1.

(B and C) RFP (red) and immunostaining for Mash1 (pseudocolored green in B) and Ki67 (pseudocolored green in C) are shown in the SVZ in coronal sections in 3 DPE mice electroporated with Scr shRNA or Rheb shRNA into NSCs at P0. pCAG-RFP was coelectroporated to label SVZ cells in both conditions. Arrowheads point to Mash1+ and Ki67+ cells. In these images, cells expressing GFP from the shRNA vector (due to the absence of Cre coexpression) were not present, allowing us to pseudocolor Alexa Fluor 633-fluorescent immunostaining in green.

(D) Bar graphs show the percentage (%) of RFP+ cells in the SVZ expressing Mash1 or Ki67 under control (Scr shRNA, black) and Rheb knockdown condition (gray).

(E) RFP (red) and immunostaining for Mash1 (green) and EdU (blue) are shown in the SVZ in coronal sections in 3 DPE mice electroporated with Scr shRNA at P0.

(F) Bar graphs show the percentage (%) of Mash1+ RFP+ cells in the SVZ expressing Ki67 or EdU under control (black) and Rheb knockdown condition (gray).

(G) Bar graphs show the percentage (%) of RFP+ cells in the SVZ expressing Mash1 or Ki67 (gray) under control (Scr shRNA, black) and Raptor knockdown condition (gray) at 7 DPE.

(H) Diagram illustrates the rapamycin protocol.

(I and J) Staining for DAPI (blue) and Mash1 (red in I) or Ki67 (red in J) in the SVZ in coronal sections of mice treated with saline or rapamycin is presented.

(K) Bar graphs show the percentage (%) of SVZ cells expressing Mash1 or Ki67 following saline (black) or rapamycin injections (gray). For the saline and rapamycin conditions, the percentages of cells were obtained with respect to the total DAPI+ (nuclear stain) cells in the SVZ along the lateral side of the lateral ventricle. Scale bars, 20 μm (B, C, I, and J) and 10 μm (E). Asterisks indicate statistical significance (**$p < 0.01$; ****$p < 0.0001$) by Student's t test. Error bars are SEM (n = 4–5 mice per condition). See also Figure S3.

both conditions (Figures 4F and 4H). At 4 DIV, NSCs generated clusters containing two or more RFP+ cells (Figures 4G and 4I). In the control condition, 80% of the two-cell clusters contained either two GFAP+ or a GFAP+ cell and a Mash1+ TAC, suggesting that NSCs underwent symmetric and asymmetric self-renewal, respectively (Figure 4J). In the hyperactive mTORC1 condition, cluster size and the percentage of RFP+ cells expressing Mash1 significantly increased, suggesting lineage amplification (Figures 4G and 4I). In addition, 81% of the two-cell clones contained two Mash1+ TACs (Figure 4J), indicating that hyperactive mTORC1 drives NSCs to terminally differentiate into TACs at the expense of self-renewal.

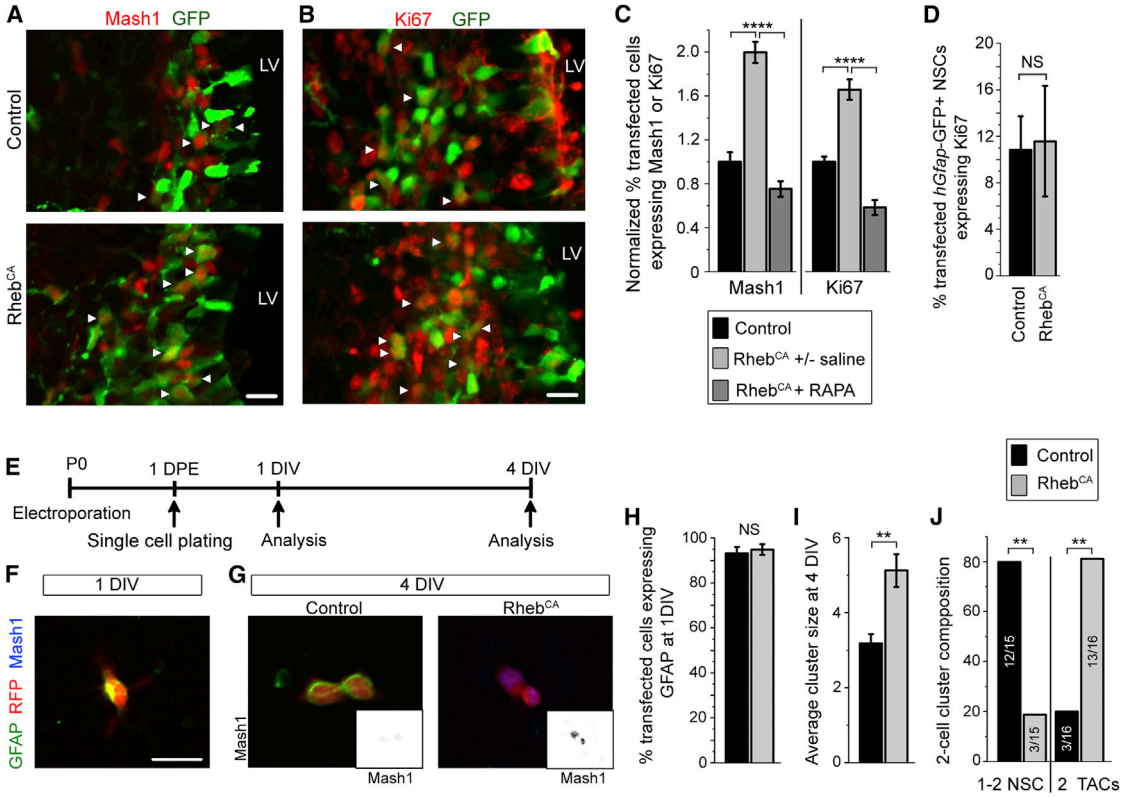

Figure 4. Increased mTORC1 Activity Drives NSC Differentiation into TACs at the Expense of Self-Renewal

(A and B) GFP (green) and immunostaining for Mash1 (red in A) and Ki67 (red in B) are shown in the SVZ in coronal sections in 3 DPE mice electroporated with RFP or Rheb^{CA} into NSCs at P0. pCAG-GFP was coelectroporated to label SVZ cells in both conditions.

(C) Bar graphs show the percentage (%) of GFP+ cells in the SVZ expressing Mash1 or Ki67 under control (black), Rheb^{CA} condition (gray), or Rheb^{CA} with rapamycin treatment (dark gray). Rheb^{CA} and Rheb^{CA} with saline gave similar results. Data were pooled.

(D) Bar graphs show the percentage (%) of transfected NSCs expressing Ki67 under control (black) and Rheb^{CA} condition (gray) at 3 DPE. For these experiments, Rheb^{CA} and RFP were electroporated in NSCs of *hGfap*-GFP mice, allowing us to distinguish NSCs from their daughter cells.

(E) Diagram illustrates the in vitro experimental protocol.

(F) Immunostaining for GFAP (green) and Mash1 (blue) is shown in RFP+ NSCs at 1 DIV that were transfected with control vector and plated 1 DPE.

(G) Immunostaining for GFAP (green) and Mash1 (blue) is presented in RFP+ two-cell clusters at 4 DIV that were transfected with either a control vector or Rheb^{CA} and plated 1 DPE. The insets illustrate Mash1 immunostaining.

(H) Bar graph shows the percentage (%) of transfected cells expressing GFAP at 1 DIV.

(I) Bar graph presents the average cluster size at 4 DIV.

(J) Bar graph shows the GFAP+ and Mash1+ cell composition of the two-cell clusters at 4 DIV.

Asterisks indicate statistical significance (**$p < 0.01$; ***$p < 0.001$; ****$p < 0.0001$) by Student's t test (C, D, H, and I) and Fisher's exact test (J) (n = 3–4 mice for each time point). Scale bars, 20 μm (A, B, and F). Error bars are SEM. See also Figure S4.

4E-BP2 Mediates mTORC1-Induced Differentiation through Cap-Dependent Translation

Finally, we aimed to better understand the mechanisms underlying mTORC1's effects on NSC differentiation. We examined the contribution of S6K1/S6K2 and 4E-BPs to mTORC1 effect on NSC differentiation and soma size (Figure 5A). S6K1/S6K2 knockdown, which reduces S6K1 and S6K2 levels in Neuro2a cells (Figures S5A and S5B), led to a reduction in the percentage of transfected SVZ cells expressing pS6 and decreased NSC soma size (Figures 5B and 5C), but it did not alter the frequency of Mash1 or Ki67 expression (Figures 5D and S5E). Consistent with these findings, coelectroporation of S6K1/S6K2 shRNA with Rheb^{CA} prevented NSC cytomegaly but not the increased frequency of Mash1+ cells and Ki67+ cells among transfected cells induced by hyperactive mTORC1 (Figures 5D and S5C).

To explore 4E-BP contribution, we employed an mTOR-resistant, constitutively active 4E-BP1 plasmid (4E-BP1^{CA}) (Figures S5C and S5D), which constitutively binds eukaryotic initiation factor 4E (eIF4E) and therefore mimics the effects of all endogenous 4EBPs. 4E-BP1^{CA} is thus expected to block cap-dependent translation induced by hyperactive mTORC1 (Choi et al., 2003). To determine whether 4E-BP1^{CA} decreased cap-dependent translation, NSCs were electroporated with a dual-luciferase reporter plasmid that encodes both *Renilla* and *firefly* luciferase. The *Renilla* luciferase is mediated by cap-dependent translation, whereas the *firefly* luciferase is mediated by an intermediate ribosome entry site (IRES). The *Renilla*/firefly luciferase luminescence was calculated at 3 DPE following vector electroporation at P0. 4E-BP1^{CA} significantly decreased cap-dependent translational activity in the SVZ by 3 DPE (Figure 5J). As

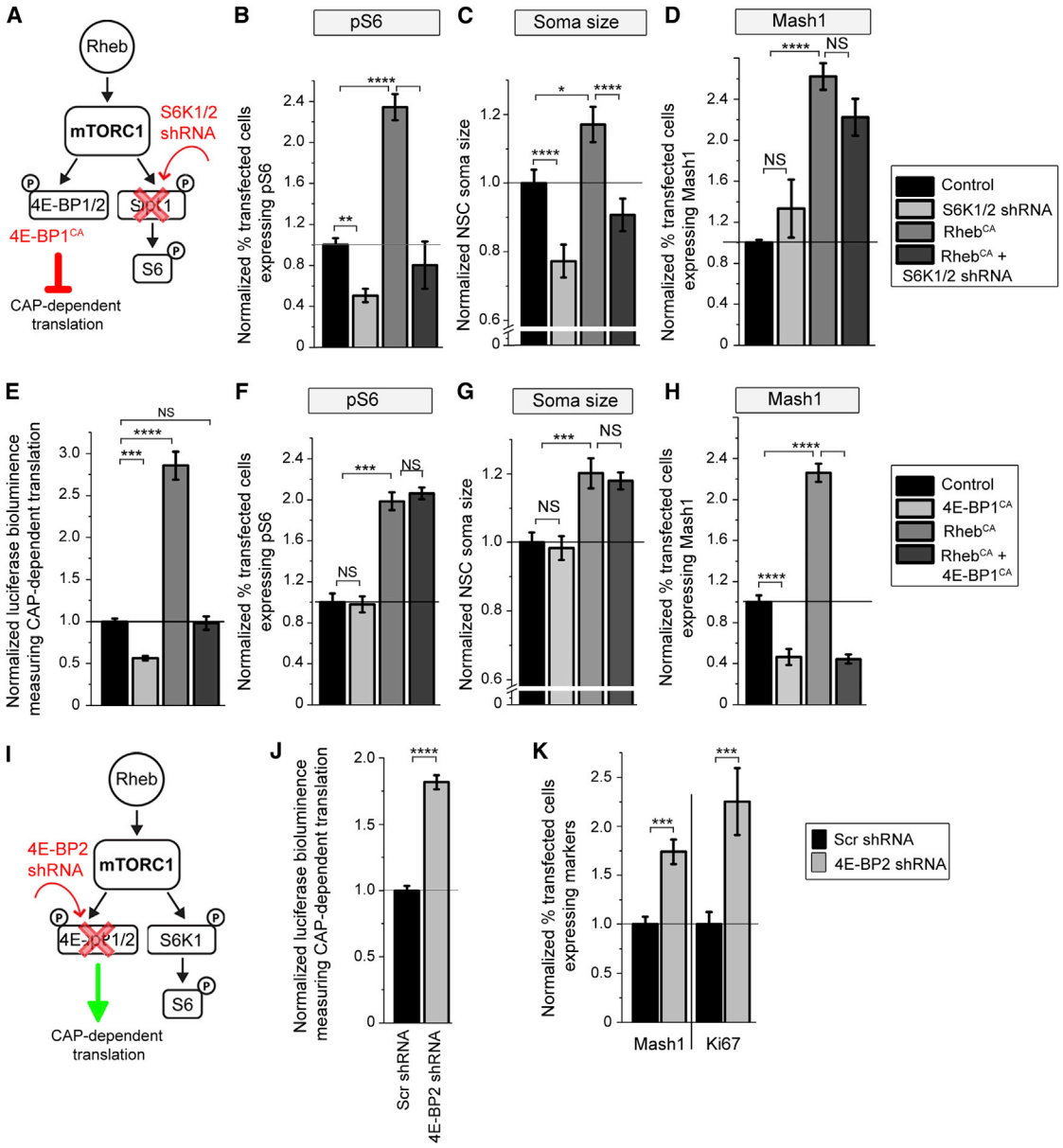

Figure 5. 4E-BP and S6K1/S6K2 Regulate NSC Differentiation and Soma Size, Respectively

(A) Diagram illustrates the site of S6K1/S6K2 shRNA and 4E-BP1^{CA} actions.

(B–D) Test shows S6K1/S6K2 shRNA alone and Rheb^{CA} condition. Bar graphs show the percentage (%) of transfected cells expressing pS6 (B), the normalized NSC soma size (C), and the normalized percentage (%) of transfected cells expressing Mash1 (D) at 3 DPE under the conditions listed in the legend on the right.

(E) Bar graph shows *Renilla/Firefly* luciferase bioluminescence to measure cap-dependent translation levels from SVZ lysates 3 days following transfection of pcDNA3-rLuc-PolioIRES-fLuc along with a vector encoding GFP (control), Rheb^{CA}, and Rheb^{CA} with 4E-BP1^{CA}.

(F–H) Test presents 4E-BP1^{CA} alone and Rheb^{CA} condition. Bar graphs show the percentage (%) of transfected cells expressing pS6 (F), the normalized NSC soma size (G), and the normalized percentage (%) of transfected cells expressing Mash1 (G) at 3 DPE under the conditions listed in the legend on the right.

(I) Diagram illustrates the site of 4E-BP2 shRNA action and consequence on cap-dependent translation.

(J) Bar graph shows *Renilla/Firefly* luciferase bioluminescence to measure cap-dependent translation levels from SVZ lysate 3 days following transfection of pcDNA3-rLuc-PolioIRES-fLuc along with a vector encoding scramble shRNA (control), 4E-BP1^{CA}, 4E-BP2 shRNA, and 4E-BP1^{CA} with 4E-BP2 shRNA.

(K) Bar graphs show the percentage (%) of RFP+ cells in the SVZ expressing Mash1 or Ki67 under control (Scr shRNA in black) and 4E-BP2 knockdown condition (gray).

Asterisks indicate statistical significance (*p < 0.05; **p < 0.01; ***p < 0.001; ****p < 0.0001) by one-way ANOVA or Student's t test (n = 3–5 mice per condition). Error bars are SEM. See also Figure S5.

expected, Rheb^{CA} had the opposite effects and significantly increased cap-dependent translational activity in the SVZ by 3 DPE (Figure 5E). Furthermore, when coexpressed with the Rheb^{CA}, 4E-BP1^{CA} was able to prevent Rheb^{CA}-induced increase in cap-dependent luciferase luminescence (Figure 5E).

In contrast to S6K1/S6K2 knockdown, electroporation of 4E-BP1^{CA} alone in NSCs at P0 did not alter pS6 expression and did not affect NSC soma size (Figures 5F and 5G). However, 4E-BP1^{CA} decreased the percentage of Mash1+ TACs and Ki67+ cells among transfected SVZ cells, similar to Rheb knockdown (Figures 5H and S5E). In addition, 4E-BP1^{CA} prevented the increased differentiation of NSCs into Mash1+ TACs and thus the Ki67+ cell generation induced by hyperactive mTORC1 (Figures 5H and S5E). Considering that 4E-BP2 is the major 4E-BP expressed in the brain (Banko et al., 2005), we explored the effect of 4E-BP2 knockdown on cap-dependent translation and NSC differentiation in vivo using a shRNA targeted against 4E-BP2 (Figures S5F and S5G). Electroporation of 4E-BP2 shRNA at P0 increased cap-dependent translational activity in the SVZ by 5 DPE as expected (Figures 5I and 5J). In addition, 4E-BP2 knockdown significantly increased the percentage of Mash1+ TACs and Ki67+ cells among transfected SVZ cells at 5 DPE, similar to the hyperactive mTORC1 condition (Figure 5K). Thus, knockdown of 4E-BP2, which leads to an increase in cap-dependent translation, is sufficient to induce NSC differentiation.

DISCUSSION

Here, we have identified the physiological function of mTORC1 on neonatal NSC self-renewal. In particular, decreased mTORC1 activity prevented NSC differentiation, leading to a reduced density of newborn neurons. In addition, we found that repression of 4E-BP activity by mTORC1, which results in an increase in cap-dependent translation, is critical for NSC self-renewal and differentiation. By contrast, mTORC1-activated S6K1/S6K2 regulated NSC size but not differentiation, indicating different functions of 4E-BPs and S6K1/S6K2 on NSCs.

To decrease mTORC1 activity, we knocked down Rheb as well as Raptor using shRNA and electroporation in neonates. This approach allowed us to selectively transfect NSCs; it is important to recognize that the transfected plasmids are passed on to the progeny of NSCs, including TACs and neuroblasts. We found that constitutive expression of Rheb shRNA in NSCs and thus TACs and neuroblasts was associated with decreased newborn neuron density in the OB examined at 14 DPE. Using a conditional shRNA vector in transgenic mice expressing Cre in neuroblasts limited Rheb shRNA expression to neuroblasts. This approach revealed that decreasing mTORC1 activity only in neuroblasts did not affect the density of newborn neurons, suggesting that decreasing mTORC1 activity in NSCs/TACs is responsible for decreased neuron production. We next dissected the effects of mTORC1 activity in NSCs by examining the frequency of transfected cells expressing the TAC marker Mash1 and the proliferative marker Ki67 at 3 DPE as well as the percentage of transfected NSCs that proliferate. In 3 days, NSCs self-renewed and generated Mash1+ TACs, most of which (>90%) are proliferative. In decreased mTORC1 condition, fewer Mash1+ cells were generated, explaining the decreased neuron production. Consistent with these data, rapamycin treatment decreased the number of Mash1+ and Ki67+ cells in the SVZ, as previously reported by Paliouras et al. (2012). However, we found that the proliferative status of Mash1+ TACs expressing Rheb shRNA was not changed, suggesting that decreased mTORC1 activity did not prevent TAC proliferation, which was previously suggested. Rather, we propose that reduced mTORC1 prevents NSC differentiation into TACs because in the hyperactive mTORC1 condition, more Mash1+ TACs were generated, and the proliferative index of transfected NSCs was not affected. Thus, mTORC1 activity does not induce NSCs to enter the cell cycle but, rather, is a regulator of their differentiation into their daughter cells: Mash1+ TACs in the neonatal SVZ. Our finding explains the loss of NSCs with aging that is associated with increased mTORC1 (Johnson et al., 2013). High levels of mTORC1 activity over time would lead to NSC terminal differentiation and thus exhaustion.

Using similar approaches, we next identified that S6K1/S6K2 regulates NSC soma size, but not differentiation. Cell size regulation is a conserved function of S6K and S6 phosphorylation (Ruvinsky and Meyuhas, 2006; Montagne et al., 1999) and is not commonly affected by 4E-BPs in mammalian cells (Dowling et al., 2010). The sole contribution of 4E-BPs, and more specifically 4E-BP2, to mTORC1-regulated NSC differentiation was unpredicted but places 4E-BP2 as a key determinant of NSC differentiation versus amplification and, thus, neuronal density and brain size. In addition, although we cannot completely rule out an increase in transcription in the Rheb^{CA} condition, the direct manipulations of 4E-BP activity suggest that cap-dependent translation, monitored by luciferase activity in vivo, is involved in regulating NSC self-renewal at baseline and under hyperactive mTORC1 condition.

The activity of mTORC1-4E-BP2 is affected by many environmental conditions or mutations in the PI3K signaling pathway in tumors and several neurological disorders (e.g., tuberous sclerosis complex, autism spectrum disorders, and hemimegalencephaly) (Dunlop and Tee, 2009; Tee and Blenis, 2005; Zoncu et al., 2011; Laplante and Sabatini, 2012; Levitt and Campbell, 2009; Lee et al., 2012). These disorders affect brain development and are associated with mild-to-severe cognitive and psychiatric impairments. We thus propose that 4E-BP2 is a target of choice for preventing or rescuing abnormal brain development in infants during perinatal life. In addition, future therapies could direct tumor differentiation by developing molecules to switch on or off 4E-BP2 activity on cap-dependent translation.

EXPERIMENTAL PROCEDURES

Animals

Research protocols were approved by the Yale University Institutional Animal Care and Use Committee. Experiments were performed on littermate wild-type CD1 mice (Charles River), and transgenic *hGfap*-GFP mice and *Dlx5*/*Dlx6*-Cre mice (The Jackson Laboratory).

Slice Preparation, Immunostaining, and Antibodies

Slice preparation and immunostaining were performed as previously described (Lafourcade et al., 2013; Feliciano et al., 2012). Primary antibodies were as follows: rabbit anti-pS6 (1:500 S240/244, no.5364; Cell Signaling); rabbit anti-p4E-BP1/BP2 (1:200 Thr37/46, no.2855; Cell Signaling); mouse

Table 1. List of Vectors

Vectors	Origin
CAG Promoter	
GFP	Addgene no.1150
tdTomato = RFP	Pathania et al. (2012)
$Rheb^{CA}$	Dr. Hanada, Tokyo (Maehama et al., 2008)
mTOR-resistant 4E-BP1 = $4E\text{-}BP1^{CA}$	synthesized the gene with a Phe^{113} to Ala point mutation previously reported in Choi et al. (2003) and inserted it into the Rheb encoding vector following excision of Rheb
A Cre/LoxP conditional RFP (pCALNL-RFP for dsRed2)	Addgene no.13769 for dsRed (Matsuda and Cepko, 2007)
Cre	Addgene no.13775
Blue fluorescent protein (BFP)	Dr. Joshua J. Breunig, Cedars-Sinai (Breunig et al., 2012)
Conditional U6 Promoter Encoding shRNA (pSico no.11578 or pSicoR no.12084; Ventura et al., 2004)	
Rheb shRNA (backbone vector)	Sigma-Aldrich/RNAi consortium, Broad institute
	target sequence, CCCGTCATCCTTGAAGATAAA
Scrambled shRNA	Young et al., 2012
Raptor shRNA	sequence from Broad Institute (Clone ID, TRCN0000077472)
S6K1/S6K2 shRNA	Target sequence, CTCAGTGAGAGTGCCAACCAA from Bae et al. (2012)
4E-BP2 shRNA	Sigma-Aldrich/RNAi consortium, Broad institute
	target sequence (Clone ID, TRCN0000321000)
Luciferase (Luc) Reporter Vector	
pcDNA3-rLuc-PolioIRES-fLuc (Renilla and firefly Luc, rLuc, and fLuc)	John Blenis (Roux et al., 2007) originally provided by Dr. Bitterman (University of Minnesota)

or rabbit anti-GFAP (1:500; Sigma-Aldrich or Dako); mouse anti-Mash1 (1:200; BD Biosciences); mouse or rabbit anti-Ki67 (1:200 or 1:250; BD Biosciences and Vector, respectively); chicken anti-GFP (1:500 ab13970; Abcam); and guinea pig anti-DCX (1:1500; Millipore). EdU staining was performed using the Click-iT Kit (Life Technologies) followed by the primary antibody staining protocol. Immunostaining of cell cultures was performed by briefly washing dishes with PBS and fixing in 4% paraformaldehyde for 15 min. After three washes in PBS, cells were blocked with 2% BSA in 0.1% PBS-Triton X-100. Cells were washed five times and incubated overnight in blocking buffer (2% BSA in PBS) at 4°C on an orbital shaker. Dishes were washed five times in PBS, and secondary antibodies in blocking buffer were added for 1 hr at room temperature. Dishes were washed five more times in PBS and counterstained with DAPI (1:5,000) for 5 min before washing three times in PBS and mounting a coverslip with ProLong Gold antifade reagent. Each staining was replicated in three to four slices from at least three different mice. Z section images were acquired on a confocal microscope (Olympus FluoView 1000) with a 20× dry objective (N.A. 0.75). Low-magnification images were acquired with a 10× dry objective or a dissecting scope (SZX16 with a 1× objective). Images were reconstructed using ImageJ 1.39t software (Wayne Rasband, NIH) or Photoshop CS3.

For pS6 and p4E-BP1/BP2 immunohistochemical analyses, identical settings for imaging were set between the two conditions, and staining above background of the no primary controls was used to identify cells as positive for either p4E-BP or pS6. The number of positive cells was then used to analyze effects of mTORC1 inhibition and hyperactivation in the SVZ.

Neonatal Electroporation

Electroporation was performed as we previously described (Platel et al., 2010; Lacar et al., 2010; Feliciano et al., 2012, 2013a). Plasmids (1–2 μg/μl) were diluted in PBS containing 0.1% fast green as a tracer. A total of 0.5–1 μl of plasmid solution was injected into the lateral ventricles of cold-anesthetized neonatal pups using a pulled glass pipette (diameter <50 μm). Five square pulses of 50 ms duration with 950 ms intervals at 100 V were applied using a pulse ECM830 BTX generator and tweezers-type electrodes (model 520; BTX) placed on the heads of P0-P1 pups.

Vectors

shRNAs were inserted into the HpaI/XhoI sites in the pSico or pSicoR vectors (Addgene; Ventura et al., 2004). A control shRNA was a scrambled sequence that did not complement any known gene using a BLAST search. pSico contains a U6 promoter preceding a Stop sequence containing enhanced GFP flanked by LoxP sites prior to the shRNA sequence. pSico was coinjected with pCAG-RFP and pCAG-Cre. The other vectors and their sources are listed in Table 1.

Cell Counts in the SVZ and In Vivo Cell Density Measurement

Z stack images of the lateral wall of the SVZ in coronal sections were acquired with a 20× dry objective using high-low settings to minimize saturation. Images were reconstructed and were manually counted for each cell marker using ImageJ 1.39t software. DAPI was routinely used as a counterstain to count the percentage of SVZ cells expressing a specific marker. Three to four sections containing the SVZ from a minimum of three mice per condition were analyzed. For cell density measurements, confocal z stacks of serial coronal sections were acquired at 10×. ImageJ (NIH) was used to count cells in a given volume to calculate cell density. Each image was adjusted for threshold and analyzed for particles greater than 20 μm^2 with a circularity between 0.5 and 1.0. All cells were counted in three different OB sections in a randomly selected series from each animal. At least three animals were analyzed per condition.

Neuro2a Cell Culture, Transfection, Western Blots, and Antibodies

The Neuro2a mouse neuroblastoma cell line (American Type Culture Collection) was propagated in tissue culture-treated polystyrene multiwell plates or flasks (Falcon; BD Biosciences Discovery Labware). The growth medium consisted of DMEM (Invitrogen) supplemented with 10% heat-inactivated fetal calf serum and penicillin-streptomycin at 100 U/l and 100 μg/l each (Invitrogen). Cells were maintained at 37°C and 5% CO_2. PolyJet (SignaGen Laboratories) was used to transfect expression vectors according to the instructions of the manufacturer when cells reached 80% confluency. For transfection of shRNA against S6K1/S6K2, nucleofection of the vectors with protocols designed by Amaxa specifically for Neuro2a cells was used. Briefly, 1.5×10^6 Neuro2a cells

per condition were resuspended in 100 μl of Nucleofector Solution and 2 μg of vector DNA. Cells were transfected using program T-024 in the Amaxa Nucleofector II and plated into three wells of a 6-well plate in Neuro2a growth media. RNA and protein were harvested 48 hr after transfection.

For western blots, samples were homogenized in 300 μl of RIPA buffer, 1× Halt Protease and phosphatase inhibitor cocktail (Thermo Fisher Scientific), and 8 U/ml DNase. Samples were boiled in 2× Laemmli's buffer for 5 min. Approximately 20 μg protein/sample was loaded into a 4%–15% polyacrylamide gel (Bio-Rad Mini Protean TGX gel). Proteins were transferred to PVDF and blocked in 5% milk or 5% BSA. When appropriate, the blots were probed for pS6 or other antibodies, stripped with Restore Western Stripping Buffer from Pierce (catalog no.21059), followed by probing for ERK1/2. All quantifications were performed using NIH ImageJ software. Antibodies for western blots included the following: anti-pS6$^{240/244}$ (1:10,000, catalog no.5368; Cell Signaling Technology); anti-Raptor (1:5,000; Cell Signaling Technology); anti-Rheb (1:5,000; Thermo Scientific); anti-pS6K1 (1:2,000; Cell Signaling); anti-S6K1 (1:3,000, catalog no.2708; Cell Signaling Technology); anti-S6K2 (1:3,000; Bethyl Laboratories); rabbit anti-4E-BP1 (1:25,000 53H11; Cell Signaling); anti-4E-BP2 (1:5,000; Cell Signaling Technology); and rabbit anti-ERK1/2 (1:20,000; Santa Cruz Biotechnology). HRP-conjugated donkey anti-rabbit from SouthernBiotech was used as secondary antibody (1:5,000).

NSC Culture

Protocols for primary NSC culture were based on previous studies by Ortega et al. (2011) and Costa et al. (2011). Briefly, P0–P1 pups were electroporated as above. Twelve hours following electroporation, pups were anesthetized, decapitated, and brains were placed in ice-cold Dissection Media (HBSS with 10 mM HEPES) and cut into 400 μm coronal sections on a vibratome. Using a No. 11 scalpel, the electroporated SVZ was dissected away from the tissue and placed into 10 ml of ice-cold Dissection Media. After a brief spin (200 × *g* for 5 min), SVZ sections were resuspended in 5 ml Dissociation Media (0.7 mg/ml trypsin and 0.7 mg/ml hyaluronidase in Solution 1 [HBSS with 2.7% glucose and 15 mM HEPES]). Sections were incubated for 30 min at 37°C with one gentle trituration at 15 min. Sections were then resuspended with 5 ml ice-cold Solution 3 (EBSS with 4% BSA and 20 mM HEPES) and passed through a 70 μm pore cell strainer. Cells were spun down at 200 × *g* for 10 min. Cells were resuspended in 10 ml ice-cold Solution 2 (HBSS with 0.9 M D-(+)-saccharose) and spun again for 10 min at 450 × *g*. Cells were resuspended in ice-cold Solution 3 and spun down at 250 × *g* for 10 min. Cells were resuspended in NSC Culture Media (DMEM/F12 supplemented with 1× B27, 1× penicillin/streptomycin, 1× GlutaMAX, and 8 mM HEPES) and plated on poly-d-lysine (1 mg/ml)-coated glass bottom dishes (MatTek; no.P35G-1.5-14-C) at 200–300 cells/mm^2. Media were changed the following day and every other thereafter.

Quantification of Cap-Dependent Translation

Experiments were as previously reported using a luciferase reporter for measuring HIF1A transcriptional activity (Feliciano et al., 2013c). Mice were electroporated with a bicistronic luciferase reporter plasmid, pcDNA3-rLuc-PolioIRES-fLuc, with pCAG-Rheb or a control pCAG-GFP vector. The reporter vector directs cap-dependent translation of the Renilla luciferase gene and the cap-independent Polio IRES-mediated translation of the firefly luciferase gene (Roux et al., 2007; Krüger et al., 2001). SVZ-containing transfected cells at 3 DPE were microdissected and flash frozen in liquid nitrogen. Samples were then placed in 0.1 ml ice-cold lysis buffer and subjected to the luciferase assay (Promega) according to the manufacturer's recommendations. Tissue was incubated in a thermomixer for 15 min, shaken at 800 rpm at 23°C. Samples were centrifuged at 10,000 × *g* for 10 min at 4°C. The supernatant was then placed on ice for ~15 min. A total of 30 μl of sample was preloaded into 100 μl of luciferase assay substrate and briefly mixed. The luminescence was measured in a TD 20/20 Luminometer (Turner Designs). Measurements were performed in duplicate or triplicate from at least four mice. Illustrated data represent the normalized luminescence from *Renilla* luciferase divided by that of *Firefly* luciferase. The different controls did not show any statistical difference, and data were pooled together (e.g., for 4E-BP1^{CA} alone and Rheb^{CA} plus 4E-BP1^{CA}).

Soma Size Measurement

To measure cell size, z stack images of RFP+ or GFP+ cells in coronal sections were acquired with a 20× dry objective (Numerical Aperture, 0.75) using high-low settings to minimize saturation. In ImageJ, the freehand tracing tool was used to outline cell somas.

Drug Treatments

Rapamycin (0.5 mg/kg) was given as intraperitoneal injections, one every other day, to wild-type P5 pups until P9 or for Rheb^{CA} rescue experiments, immediately following electroporation, and every other day until sacrifice. EdU was dissolved in DMSO, diluted to 5% DMSO 20 mg/ml EdU in PBS, and given as intraperitoneal injections (50 mg/kg) 2 hr prior to sacrifice.

Statistics

Data were presented in Origin 8.0. Statistical significance was determined using unpaired Student's t test, one-way ANOVA, or Fisher's exact test with $p < 0.05$ for significance (KyPlot 2.0 or GraphPad Prism). Data are presented as mean ± SEM.

SUPPLEMENTAL INFORMATION

Supplemental Information includes Supplemental Experimental Procedures and five figures and can be found with this article online at http://dx.doi.org/10.1016/j.celrep.2013.09.017.

ACKNOWLEDGMENTS

This work was supported by grants from the Connecticut Stem Cell Research Program (to A.B.). We thank Drs. Hanada and Maehama (Department of Biochemistry and Cell Biology, National Institute of Infectious Diseases, Tokyo) for the Rheb^{CA} vector, Dr. Josh Breunig for the BFP-encoding vector, and Dr. Blenis (Department of Cell Biology, Harvard Medical School) for the Luciferase reporter originally generated by Dr. Bitterman (Department of Medicine, University of Minnesota Medical School).

Received: April 29, 2013
Revised: August 14, 2013
Accepted: September 11, 2013
Published: October 17, 2013

REFERENCES

Bae, E.J., Xu, J., Oh, D.Y., Bandyopadhyay, G., Lagakos, W.S., Keshwani, M., and Olefsky, J.M. (2012). Liver-specific p70 S6 kinase depletion protects against hepatic steatosis and systemic insulin resistance. J. Biol. Chem. *287*, 18769–18780.

Banko, J.L., Poulin, F., Hou, L., DeMaria, C.T., Sonenberg, N., and Klann, E. (2005). The translation repressor 4E-BP2 is critical for eIF4F complex formation, synaptic plasticity, and memory in the hippocampus. J. Neurosci. *25*, 9581–9590.

Boutin, C., Diestel, S., Desoeuvre, A., Tiveron, M.C., and Cremer, H. (2008). Efficient in vivo electroporation of the postnatal rodent forebrain. PLoS One *3*, e1883.

Breunig, J.J., Gate, D., Levy, R., Rodriguez, J., Jr., Kim, G.B., Danielpour, M., Svendsen, C.N., and Town, T. (2012). Rapid genetic targeting of pial surface neural progenitors and immature neurons by neonatal electroporation. Neural Dev. *7*, 26.

Chesler, A.T., Le Pichon, C.E., Brann, J.H., Araneda, R.C., Zou, D.J., and Firestein, S. (2008). Selective gene expression by postnatal electroporation during olfactory interneuron neurogenesis. PLoS One *3*, e1517.

Choi, K.M., McMahon, L.P., and Lawrence, J.C., Jr. (2003). Two motifs in the translational repressor PHAS-I required for efficient phosphorylation by mammalian target of rapamycin and for recognition by raptor. J. Biol. Chem. *278*, 19667–19673.

Chong, Z.Z., Shang, Y.C., Zhang, L., Wang, S., and Maiese, K. (2010). Mammalian target of rapamycin: hitting the bull's-eye for neurological disorders. Oxid. Med. Cell. Longev. *3*, 374–391.

Costa, M.R., Ortega, F., Brill, M.S., Beckervordersandforth, R., Petrone, C., Schroeder, T., Götz, M., and Berninger, B. (2011). Continuous live imaging of adult neural stem cell division and lineage progression in vitro. Development *138*, 1057–1068.

Dowling, R.J., Topisirovic, I., Alain, T., Bidinosti, M., Fonseca, B.D., Petroulakis, E., Wang, X., Larsson, O., Selvaraj, A., Liu, Y., et al. (2010). mTORC1-mediated cell proliferation, but not cell growth, controlled by the 4E-BPs. Science *328*, 1172–1176.

Dunlop, E.A., and Tee, A.R. (2009). Mammalian target of rapamycin complex 1: signalling inputs, substrates and feedback mechanisms. Cell. Signal. *21*, 827–835.

Ehninger, D., and Silva, A.J. (2011). Rapamycin for treating Tuberous sclerosis and Autism spectrum disorders. Trends Mol. Med. *17*, 78–87.

Feliciano, D.M., Quon, J.L., Su, T., Taylor, M.M., and Bordey, A. (2012). Postnatal neurogenesis generates heterotopias, olfactory micronodules and cortical infiltration following single-cell Tsc1 deletion. Hum. Mol. Genet. *21*, 799–810.

Feliciano, D.M., Lafourcade, C.A., and Bordey, A. (2013a). Neonatal subventricular zone electroporation. J. Vis. Exp. (72), 50197.

Feliciano, D.M., Lin, T.V., Hartman, N.W., Bartley, C.M., Kubera, C., Hsieh, L., Lafourcade, C., O'Keefe, R.A., and Bordey, A. (2013b). A circuitry and biochemical basis for tuberous sclerosis symptoms: from epilepsy to neurocognitive deficits. Int. J. Dev. Neurosci. Published online February 26, 2013. http://dx.doi.org/10.1016/j.ijdevneu.2013.02.008.

Feliciano, D.M., Zhang, S., Quon, J.L., and Bordey, A. (2013c). Hypoxia-inducicle factor 1a is a *Tsc1*-regulated survival factor in newborn neurons in tuberous sclerosis complex. Hum. Mol. Genet. *22*, 1725–1734.

Gage, F.H. (2000). Mammalian neural stem cells. Science *287*, 1433–1438.

Hoeffer, C.A., and Klann, E. (2010). mTOR signaling: at the crossroads of plasticity, memory and disease. Trends Neurosci. *33*, 67–75.

Hoeffer, C.A., Sanchez, E., Hagerman, R.J., Mu, Y., Nguyen, D.V., Wong, H., Whelan, A.M., Zukin, R.S., Klann, E., and Tassone, F. (2012). Altered mTOR signaling and enhanced CYFIP2 expression levels in subjects with fragile X syndrome. Genes Brain Behav. *11*, 332–341.

Inoki, K., Corradetti, M.N., and Guan, K.L. (2005). Dysregulation of the TSC-mTOR pathway in human disease. Nat. Genet. *37*, 19–24.

Johnson, S.C., Rabinovitch, P.S., and Kaeberlein, M. (2013). mTOR is a key modulator of ageing and age-related disease. Nature *493*, 338–345.

Kohwi, M., Petryniak, M.A., Long, J.E., Ekker, M., Obata, K., Yanagawa, Y., Rubenstein, J.L., and Alvarez-Buylla, A. (2007). A subpopulation of olfactory bulb GABAergic interneurons is derived from Emx1- and Dlx5/6-expressing progenitors. J. Neurosci. *27*, 6878–6891.

Krüger, M., Beger, C., Welch, P.J., Barber, J.R., Manns, M.P., and Wong-Staal, F. (2001). Involvement of proteasome alpha-subunit PSMA7 in hepatitis C virus internal ribosome entry site-mediated translation. Mol. Cell. Biol. *21*, 8357–8364.

Lacar, B., Young, S.Z., Platel, J.C., and Bordey, A. (2010). Imaging and recording subventricular zone progenitor cells in live tissue of postnatal mice. Front. Neurosci. *4*, 43.

Lafourcade, C.A., Lin, T.V., Feliciano, D.M., Zhang, L., Hsieh, L.S., and Bordey, A. (2013). Rheb activation in subventricular zone progenitors leads to heterotopia, ectopic neuronal differentiation, and rapamycin-sensitive olfactory micronodules and dendrite hypertrophy of newborn neurons. J. Neurosci. *33*, 2419–2431.

Lamming, D.W., Ye, L., Sabatini, D.M., and Baur, J.A. (2013). Rapalogs and mTOR inhibitors as anti-aging therapeutics. J. Clin. Invest. *123*, 980–989.

Laplante, M., and Sabatini, D.M. (2012). mTOR signaling in growth control and disease. Cell *149*, 274–293.

Lee, J.H., Huynh, M., Silhavy, J.L., Kim, S., Dixon-Salazar, T., Heiberg, A., Scott, E., Bafna, V., Hill, K.J., Collazo, A., et al. (2012). De novo somatic mutations in components of the PI3K-AKT3-mTOR pathway cause hemimegalencephaly. Nat. Genet. *44*, 941–945.

Levitt, P., and Campbell, D.B. (2009). The genetic and neurobiologic compass points toward common signaling dysfunctions in autism spectrum disorders. J. Clin. Invest. *119*, 747–754.

Maehama, T., Tanaka, M., Nishina, H., Murakami, M., Kanaho, Y., and Hanada, K. (2008). RalA functions as an indispensable signal mediator for the nutrient-sensing system. J. Biol. Chem. *283*, 35053–35059.

Magri, L., and Galli, R. (2013). mTOR signaling in neural stem cells: from basic biology to disease. Cell. Mol. Life Sci. *70*, 2887–2898.

Magri, L., Cambiaghi, M., Cominelli, M., Alfaro-Cervello, C., Cursi, M., Pala, M., Bulfone, A., Garcìa-Verdugo, J.M., Leocani, L., Minicucci, F., et al. (2011). Sustained activation of mTOR pathway in embryonic neural stem cells leads to development of tuberous sclerosis complex-associated lesions. Cell Stem Cell *9*, 447–462.

Matsuda, T., and Cepko, C.L. (2007). Controlled expression of transgenes introduced by in vivo electroporation. Proc. Natl. Acad. Sci. USA *104*, 1027–1032.

Merkle, F.T., and Alvarez-Buylla, A. (2006). Neural stem cells in mammalian development. Curr. Opin. Cell Biol. *18*, 704–709.

Mitchell, B.D., Emsley, J.G., Magavi, S.S., Arlotta, P., and Macklis, J.D. (2004). Constitutive and induced neurogenesis in the adult mammalian brain: manipulation of endogenous precursors toward CNS repair. Dev. Neurosci. *26*, 101–117.

Montagne, J., Stewart, M.J., Stocker, H., Hafen, E., Kozma, S.C., and Thomas, G. (1999). Drosophila S6 kinase: a regulator of cell size. Science *285*, 2126–2129.

Ortega, F., Costa, M.R., Simon-Ebert, T., Schroeder, T., Götz, M., and Berninger, B. (2011). Using an adherent cell culture of the mouse subependymal zone to study the behavior of adult neural stem cells on a single-cell level. Nat. Protoc. *6*, 1847–1859.

Paliouras, G.N., Hamilton, L.K., Aumont, A., Joppé, S.E., Barnabé-Heider, F., and Fernandes, K.J. (2012). Mammalian target of rapamycin signaling is a key regulator of the transit-amplifying progenitor pool in the adult and aging forebrain. J. Neurosci. *32*, 15012–15026.

Parras, C.M., Galli, R., Britz, O., Soares, S., Galichet, C., Battiste, J., Johnson, J.E., Nakafuku, M., Vescovi, A., and Guillemot, F. (2004). Mash1 specifies neurons and oligodendrocytes in the postnatal brain. EMBO J. *23*, 4495–4505.

Pastrana, E., Cheng, L.C., and Doetsch, F. (2009). Simultaneous prospective purification of adult subventricular zone neural stem cells and their progeny. Proc. Natl. Acad. Sci. USA *106*, 6387–6392.

Pathania, M., Torres-Reveron, J., Yan, L., Kimura, T., Lin, T.V., Gordon, V., Teng, Z.Q., Zhao, X., Fulga, T.A., Van Vactor, D., and Bordey, A. (2012). miR-132 enhances dendritic morphogenesis, spine density, synaptic integration, and survival of newborn olfactory bulb neurons. PLoS One *7*, e38174.

Platel, J.C., Gordon, V., Heintz, T., and Bordey, A. (2009). GFAP-GFP neural progenitors are antigenically homogeneous and anchored in their enclosed mosaic niche. Glia *57*, 66–78.

Platel, J.C., Dave, K.A., Gordon, V., Lacar, B., Rubio, M.E., and Bordey, A. (2010). NMDA receptors activated by subventricular zone astrocytic glutamate are critical for neuroblast survival prior to entering a synaptic network. Neuron *65*, 859–872.

Roux, P.P., Shahbazian, D., Vu, H., Holz, M.K., Cohen, M.S., Taunton, J., Sonenberg, N., and Blenis, J. (2007). RAS/ERK signaling promotes site-specific ribosomal protein S6 phosphorylation via RSK and stimulates cap-dependent translation. J. Biol. Chem. *282*, 14056–14064.

Ruvinsky, I., and Meyuhas, O. (2006). Ribosomal protein S6 phosphorylation: from protein synthesis to cell size. Trends Biochem. Sci. *31*, 342–348.

Sanai, N., Nguyen, T., Ihrie, R.A., Mirzadeh, Z., Tsai, H.H., Wong, M., Gupta, N., Berger, M.S., Huang, E., Garcia-Verdugo, J.M., et al. (2011). Corridors of migrating neurons in the human brain and their decline during infancy. Nature *478*, 382–386.

Santini, E., and Klann, E. (2011). Dysregulated mTORC1-dependent translational control: from brain disorders to psychoactive drugs. Front. Behav. Neurosci. *5*, 76.

Shi, Y., Sun, G., Zhao, C., and Stewart, R. (2008). Neural stem cell self-renewal. Crit. Rev. Oncol. Hematol. *65*, 43–53.

Tee, A.R., and Blenis, J. (2005). mTOR, translational control and human disease. Semin. Cell Dev. Biol. *16*, 29–37.

Ventura, A., Meissner, A., Dillon, C.P., McManus, M., Sharp, P.A., Van Parijs, L., Jaenisch, R., and Jacks, T. (2004). Cre-lox-regulated conditional RNA interference from transgenes. Proc. Natl. Acad. Sci. USA *101*, 10380–10385.

Wang, H., and Doering, L.C. (2013). Reversing autism by targeting downstream mTOR signaling. Front. Cell. Neurosci. *7*, 28.

Young, S.Z., Taylor, M.M., Wu, S., Ikeda-Matsuo, Y., Kubera, C., and Bordey, A. (2012). NKCC1 knockdown decreases neuron production through GABA(A)-regulated neural progenitor proliferation and delays dendrite development. J. Neurosci. *32*, 13630–13638.

Zoncu, R., Efeyan, A., and Sabatini, D.M. (2011). mTOR: from growth signal integration to cancer, diabetes and ageing. Nat. Rev. Mol. Cell Biol. *12*, 21–35.